

1 Angle-resolved cathodoluminescence spectroscopy

2 Toon Coenen,^{a)} Ernst Jan R. Vesseur, and Albert Polman

3 *Center for Nanophotonics, FOM Institute AMOLF, Science Park 104, 1098 XG Amsterdam, The Netherlands*

5 (Received 18 July 2011; accepted 10 September 2011; published online xx xx xxxx)

6 We present a cathodoluminescence spectroscopy technique which combines deep subwavelength
7 excitation resolution with angle-resolved detection capabilities. The cathodoluminescence emission
8 is collected by a paraboloid mirror (effective $NA = 0.96$) and is projected onto a 2D CCD array.
9 The azimuthal and polar emission pattern is directly deduced from the image. As proof of principle,
10 we use the technique to measure the angular distribution of transition radiation from a single
11 crystalline gold surface under 30 keV electron irradiation. We find that the experiment matches
12 very well with theory, illustrating the potential of this technique for the characterization of photonic
13 structures with deep subwavelength dimensions. © 2011 American Institute of Physics.
14 [doi:10.1063/1.3644985]

15 In nanophotonics, the research field concerned with the
16 manipulation of light at the nanoscale, basic building blocks
17 like waveguides,¹ nanoantennas,² and nanocavities,³ often
18 have subwavelength geometrical features. Optical phenom-
19 ena in these structures cannot be resolved with far-field opti-
20 cal microscopy due to Abbe's law of diffraction that
21 provides a limit to the smallest distance over which individ-
22 ual objects can be distinguished. Several spatially resolved
23 spectroscopy techniques have been developed to reach a
24 resolution below that limit, including scanning near-field
25 optical microscopy (SNOM),⁴ stimulated emission depletion
26 (STED) microscopy,⁵ photoactivatable localization micros-
27 copy (PALM),⁶ and stochastic optical reconstruction micros-
28 copy (STORM).⁷

29 Cathodoluminescence (CL) imaging spectroscopy is a
30 technique that has even higher spatial resolution, as it uses
31 an electron beam as an excitation source. In
32 CL-spectroscopy, an electron beam focused to a 1-10 nm
33 spot is raster scanned over a sample. The electron beam
34 effectively acts as a supercontinuum light source that excites
35 the sample according to the local density of optical states
36 (LDOS).^{8,9} Previous work has shown that CL imaging spec-
37 troscopy is a powerful technique for probing (nano)photonic
38 environments. In particular, in the field of plasmonics, where
39 large spatial variations in the LDOS can occur on deep sub-
40 wavelength length scales, CL-spectroscopy has proven to be
41 an important characterization technique.^{2,10,11}

42 So far, the CL technique was limited to measuring spec-
43 tral response as a function of excitation position, and no in-
44 formation about the total angular distribution of the CL
45 emission could be collected. Yamamoto and coworkers
46 developed a technique by which the angular distribution of
47 CL was measured by translating a pinhole in front of a CCD
48 camera, thus collecting point-by-point angular data.^{12,13}
49 In this letter, we present a further advanced experimental
50 technique to resolve the angular distribution of CL emission,
51 in both the azimuthal and polar directions. We demonstrate
52 the technique by measuring angle-resolved transition

radiation (TR) spectra for a single-crystal Au substrate and
find an excellent agreement between experiment and theory.

Figure 1(a) shows a schematic overview of the experi-
mental setup that uses a FEI XL-30 SFEG scanning electron
microscope (SEM). For CL experiments, a diamond-turned
aluminum off-axis paraboloid mirror with a focal distance of
0.5 mm is mounted in the vacuum chamber of the micro-
scope. Directly above its focal point, this paraboloid has a
600- μm -diameter hole through which a 30 keV electron
beam can reach the sample. The CL emission is collected
by the mirror and redirected out of the SEM through a glass
vacuum flange. The beam emanating from the paraboloid is
projected onto a Peltier-cooled (-70°C) 1024×1024 pixels
back-illuminated silicon CCD camera. An achromatic lens
(focal distance 11 cm) ensures that the beam fully fills the

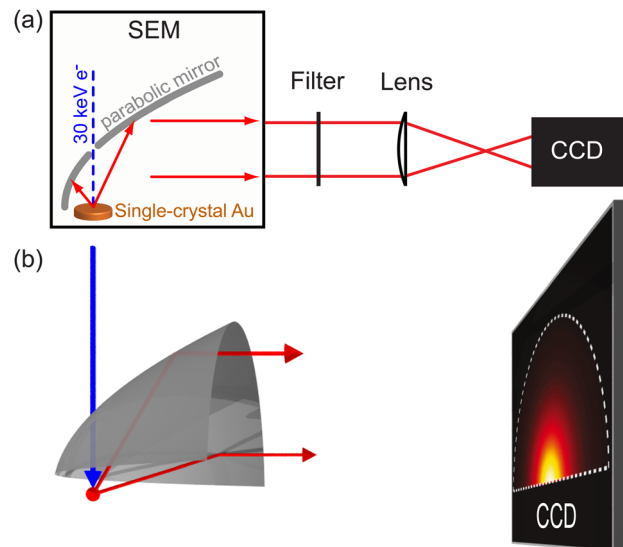


FIG. 1. (Color online) (a) Schematic overview of the experimental setup. The scanning electron microscope contains the paraboloid mirror which collects the CL-emission and redirects it towards the CCD detector. The 30 keV electron beam reaches the sample through a hole in the mirror. The lens in the setup projects the output on a 1024×1024 pixel CCD camera. From the image, the angular distribution of cathodoluminescence emission is directly determined. (b) 3D representation of how the paraboloid beam is projected onto the CCD array for an isotropic light source.

^{a)}Author to whom correspondence should be addressed. Electronic mail: coenen@amolf.nl.

68 CCD array. Color filters and polarizers can be put in the
69 beam path to add wavelength and polarization sensitivity to
70 the setup.

71 For optimum detection efficiency, the electron beam
72 must hit the sample in the focus of the mirror which requires
73 accurate positioning of the mirror relative to the sample. The
74 vertical distance between sample and mirror can be adjusted
75 accurately with the SEM stage. Micro positioning of the mir-
76 ror is done by four piezoelectric stepper motors integrated
77 with a titanium leaf spring mechanism to which the mirror is
78 attached, allowing translational (x,y) and rotational position-
79 ing (tilt and yaw) of the mirror. If the mirror is well-focused,
80 each pixel in the CCD image of the beam corresponds to a
81 single point on the paraboloid. Furthermore, each point in
82 the paraboloid is associated with a unique emission angle
83 which can be described by a zenithal angle θ running from
84 0° to 90° (where $\theta=0$ is normal to the surface) and an azi-
85 muthal angle ϕ running from 0 to 360° . This collection ge-
86 ometry is very similar to a Fourier microscope where the
87 back aperture of a microscope objective is imaged with a
88 camera to determine angular radiation patterns.⁵ Figures 2(a)
89 and 2(b) show how each pixel in the image is mapped onto
90 angles θ and ϕ , calculated using the known geometrical
91 properties of the paraboloid. Figure 2(c) shows the solid
92 angle covered per pixel which is used to correct the data to
93 photon flux per unit of solid angle. Integrating over all pixels
94 that fall within the beam gives a total acceptance angle of
95 1.46π sr, equivalent to a NA = 0.96 for a microscope objec-
96 tive. Taking only the half space left of the electron beam
97 (see Fig. 1), the solid angle is 0.96π sr, i.e., 96% of the radi-
98 ation; the remaining 4% leaves through the small opening
99 between mirror and sample. Since we have the ability to
100 rotate the sample by 180° , we can almost entirely reconstruct
101 the emission pattern for the upper hemisphere, corresponding
102 to an NA of 0.999.

103 When an electron passes through an interface between
104 two dielectric environments, it induces a dipole moment on
105 the surface which radiates into the far field (TR). The TR
106 radiation pattern is very similar to that of a vertical point
107 dipole on a surface.⁸ To test the angle-resolving capabilities
108 of the setup, we measured the TR emission from a polished
109 single-crystalline Au (100) surface irradiated with 30 keV
110 electrons over the full spectral band of the CCD. A CCD
111 image is recorded with a collection time of only 10 s. The
112 CCD-array pixels were binned twice to further improve the
113 signal-to-noise ratio. For each measurement, we collected an
114 additional image with the electron beam blanked as a refer-
115 ence. Subsequently, this signal was subtracted from the TR-
116 measurement to remove dark counts from the CCD and sig-
117 nal originating from other sources than the sample.

118 Figure 2(d) shows a CCD image obtained using the
119 method described above. The semicircular shape of the para-
120 boloid end face can clearly be recognized. The dark concen-
121 tric rings in the image are caused by radial imperfections in
122 the mirror which are inherent to the diamond turning fabrica-
123 tion process of the mirror. Also, the hole in the mirror is visi-
124 ble close to the center of the beam. The area around the hole
125 corresponds to emission angles that are almost normal to the
126 surface. This area is relatively dark, while other parts corre-
127 sponding to more grazing angles appear to be brighter (see

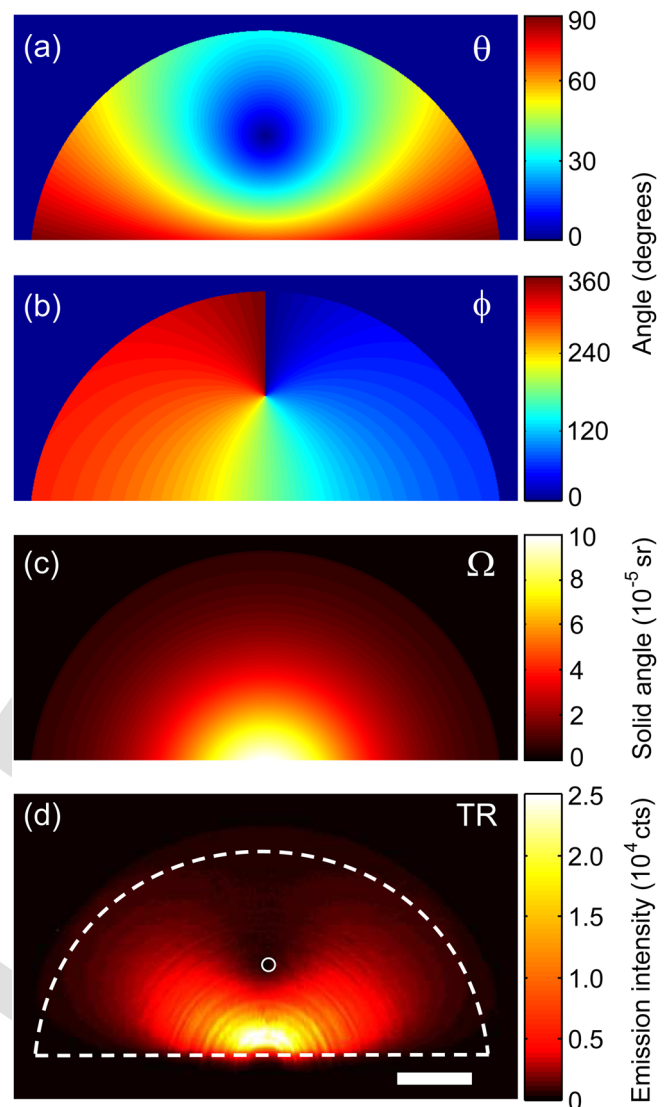


FIG. 2. (Color online) Maps relating pixel position in the CCD image to (a) polar angle θ , (b) azimuthal angle ϕ , and (c) the solid angle per pixel, allowing conversion to an absolute radiation pattern. (d) CCD image showing the measured transition radiation from a single-crystalline gold sample. The white dashed line indicates the mirror contour, and the white circle indicates the position of the hole in the mirror. The scale bar is 2 mm which corresponds to 154 CCD pixels.

Fig. 2(a)). This particular pattern in the CCD image points
towards a toroidally shaped emission pattern as predicted for
transition radiation.

Figure 3 shows the probability of exciting a TR photon
on a gold surface integrated over the entire upper hemi-
sphere, which was calculated using the theory described in
Ref. 9 and tabulated optical constants.¹⁴ Broadband emission
is expected in the 350-950 nm spectral band, with a dip
around 500 nm which is related to the plasmon resonance
frequency in gold. Integrating the probability of TR emission
from 350 to 950 nm, we find a generation rate of 1×10^{-4}
photons per incident electron. In this experiment, a current
of 12 nA was used which should then generate 8×10^6 pho-
tons s^{-1} . Taking into account the acceptance angle of the
mirror, known reflection losses in the optics, and the quan-
tum efficiency of the CCD camera, we expect $\sim 4 \times 10^6$ pho-
tons s^{-1} to be detected by the CCD camera. Integrating over

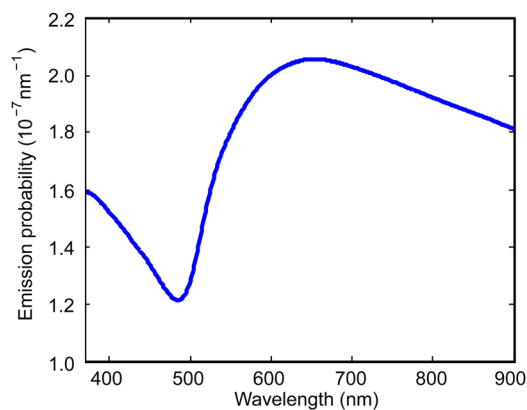


FIG. 3. (Color online) TR emission probability per incoming 30 keV e/nm bandwidth as a function of wavelength for the entire upper hemisphere calculated for a gold substrate.

145 all pixels in Fig. 2(d) and correcting for the analog gain ($4\times$)
 146 of the CCD-array, we find a collection rate of 3.9×10^6 photons
 147 s^{-1} ; similar to the calculated value. This indicates that
 148 the angle-resolved CL technique provides an accurate absolute
 149 measurement of the emitted radiation intensity.

150 To investigate the directionality of the emission in more
 151 detail, the CCD image in Fig. 2(d) was converted into a radiation
 152 pattern using the conversion maps shown in Figs.
 153 2(a)–2(c). The data were interpolated to yield points that are
 154 equally spaced in θ and ϕ . Figure 4(a) shows the angular
 155 distribution of TR emission mapped onto a polar grid where the
 156 radius represents polar angle θ , and the polar plot angle represents
 157 azimuthal angle ϕ . Fig. 4(b) shows the calculated angular
 158 distribution for 30 keV electron beam excitation integrated over the
 159 spectral sensitivity band of the CCD camera (350–950 nm). Data for
 160 angles that are not collected by the mirror are set to zero (black).
 161 CL emission close to the surface normal (around $\theta=0^\circ$) is not
 162 collected because of the hole in the mirror. Radiation emitted
 163 almost grazing to the surface ($\theta > 85^\circ$) is also not collected
 164 because of the small space between mirror and sample (0.5 mm).
 165 The largest loss in acceptance angle, clearly visible in the upper
 166 part of Figs. 4(a) and 4(b), corresponds to the open part of the
 167 paraboloid through which light is directed to the CCD camera.
 168 The experiment clearly shows a toroidal emission pattern, in
 169 good agreement with calculation. Indeed, the radiation pattern
 170 is very similar to that of a vertically oriented point dipole located
 171 close to a reflective surface.⁴

172
 173 Next, we investigate the wavelength dependence of the
 174 angular radiation pattern. Band pass filters (40 nm) were
 175 placed in the beam path with center wavelengths ranging from
 176 400 nm to 900 nm in steps of 50 nm, and angle-resolved
 177 emission patterns were measured at each wavelength. For these
 178 measurements, an integration time of 120 s was used to enable
 179 accurate measurements at 900 nm where the sensitivity of the
 180 CCD detector is lowest. To accurately compare experiment and
 181 theory, the angle-resolved emission patterns were integrated
 182 over azimuthal angle ϕ . Data in the range $\theta = 60^\circ$ for 400 nm
 183 and around $\theta = 70^\circ$ for 900 nm is clearly observed.
 184
 185
 186
 187

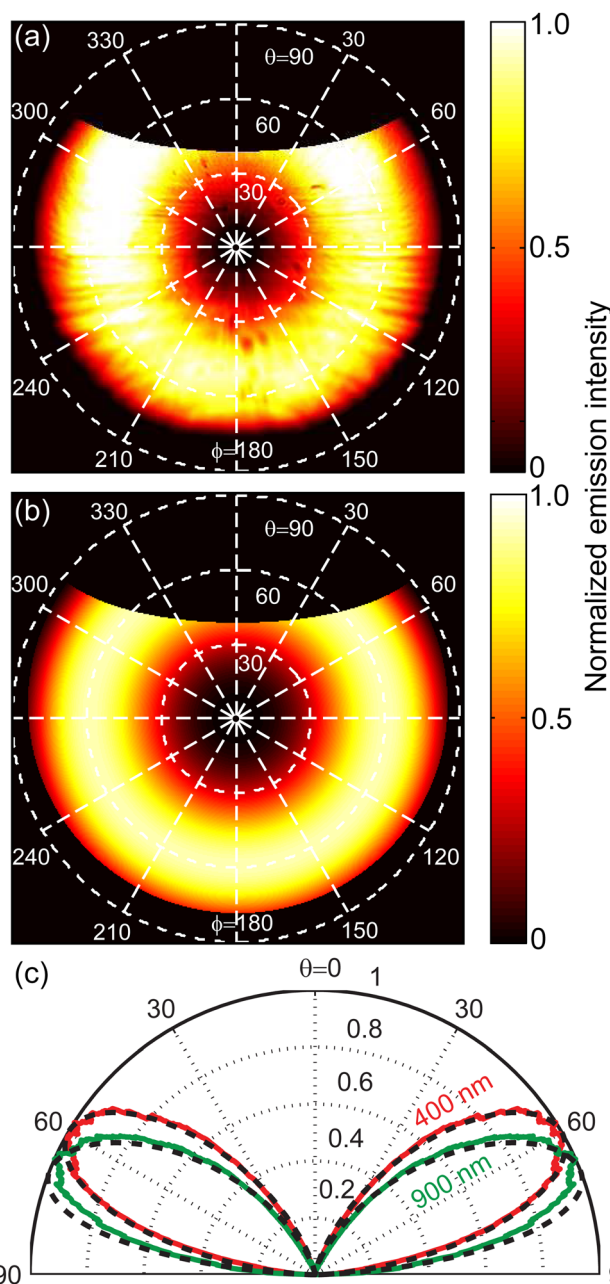


FIG. 4. (Color online) Angle-resolved cathodoluminescence emission patterns of the transition radiation for single-crystalline Au (30 keV e^-). (a) Normalized measured emission pattern collected without color filter showing the total emission intensity (350–950 nm) as a function of emission angles θ and ϕ . (b) Normalized calculated emission pattern for the same spectral range as in (a). (c) Emission pattern integrated over ϕ for transition radiation at 400 and 900 nm (red, green) and theory (black dashed lines).

lar angle θ . Figure 4(c) shows the normalized CL intensity as
 188 function of θ for 400 nm (red curve) and 900 nm (green
 189 curve) together with theoretically predicted emission pat-
 190 terns (black dashed curves). We find excellent agreement
 191 between experiment and theory. The overall shape of the
 192 lobes is well reproduced, and the small difference in lobe
 193 orientation between these wavelengths (peak emission around
 194 $\theta = 60^\circ$ for 400 nm and around $\theta = 70^\circ$ for 900 nm) is clearly
 195 observed.
 196

In conclusion, we have presented an experimental tech-
 197 nique for angle-resolved cathodoluminescence spectroscopy.
 198 We determined the angular distribution of transition radi-
 199 ation from a single crystal gold substrate and found that the
 200

AQ1

201 experimental results agree very well with theory. A photon
 202 count rate in the order of 10^6 photons s^{-1} is observed, corre-
 203 sponding closely to the calculated value. The mirror collec-
 204 tion geometry corresponds to an effective $NA = 0.96$.
 205 Combining the angle resolved capabilities with the high spa-
 206 tial excitation resolution of electron microscopy makes this
 207 cathodoluminescence technique an interesting tool for study-
 208 ing a wealth of optical phenomena in a wide variety of pho-
 209 tonic nanostructures.

210 We would like to thank Hans Zeijlemaker, Iliya Cerjak,
 211 and Johan Derks for their technical support. This work is a
 212 part of the research program of the “Stichting voor Funda-
 213 menteel Onderzoek der Materie (FOM),” which is financially
 214 supported by the “Nederlandse Organisatie voor Weten-
 215 schappelijk Onderzoek (NWO).” This work is also a part of
 216 NanoNextNL, a nanotechnology program funded by the
 217 Dutch ministry of economic affairs.
 218

- ¹E. Verhagen, M. Spasenović, A. Polman, and L. Kuipers, *Phys. Rev. Lett.* **219**
102, 203904 (2009). **220**
- ²E. J. R. Vesseur, J. García de Abajo, and A. Polman, *Nano Lett.* **221**
9, 3147 (2009). **222**
- ³L. Novotny and N. F. van Hulst, *Nat. Photonics* **5**, 83 (2011). **223**
- ⁴L. Novotny and B. Hecht, *Principles of Nano-Optics* (Cambridge Univer- **224**
sity press, New York, 2006). **225**
- ⁵V. Westphal and S. W. Hell, *Phys. Rev. Lett.* **94**, 143903 (2005). **226**
- ⁶E. Betzig, G. H. Patterson, R. Sougrat, O. W. Lindwasser, S. Olenych, **227**
J. S. Bonifacino, M. W. Davidson, J. Lippincott-Schwartz, and H. F. Hess, **228**
Science **313**, 1642 (2006). **229**
- ⁷M. Rust, M. Bates, and X. Zhuang, *Nat. Methods* **3**, 793 (2006). **230**
- ⁸M. Kuttge, E. J. R. Vesseur, A. F. Koenderink, H. J. Lezec, H. A. Atwater, **231**
F. J. García de Abajo, and A. Polman, *Phys. Rev. B* **79**, 113405 (2009). **232**
- ⁹F. J. García de Abajo, *Rev. Mod. Phys.* **82**, 209 (2010). **233**
- ¹⁰M. Kuttge, F. J. García de Abajo, and A. Polman, *Nano Lett.* **10**, 1537 **234**
(2009). **235**
- ¹¹N. Yamamoto, S. Ohtani, and F. J. García de Abajo, *Nano Lett.* **11**, 91 **236**
(2011). **237**
- ¹²T. Suzuki and N. Yamamoto, *Opt. Express* **17**, 23664 (2009). **238**
- ¹³K. Takeuchi and N. Yamamoto, *Opt. Express* **19**, 12365 (2011). **239**
- ¹⁴P. B. Johnson and R. W. Christy, *Phys. Rev. B* **6**, 4370 (1972). **240**